AIAA JOURNAL
Vol. 38, No. 10, October 2000

Shear Layer Flapping and Interface Convolution in a Separated Supersonic Flow

C. J. Bourdon* and J. C. Dutton†
University of Illinois at Urbana–Champaign, Urbana, Illinois 61801

The steadiness and convolution of the interface between the freestream and recirculating/wake core regions in an axisymmetric, separated supersonic flow were studied using planar imaging. Five regions along the shear layer/wake boundary were investigated in detail to quantify the effects that key phenomena, such as the recompression and reattachment processes, have on the development of large-scale unsteady motions and interfacial convolution. These studies show that flapping motions, when viewed from the side, generally increase in magnitude, in relation to the local shear layer thickness, with downstream distance, except at the mean reattachment point, where they are slightly suppressed. When viewed from the end, the area-based (pulsing) fluctuations increase monotonically downstream as a percentage of the local area, whereas the position-based (flapping) motions show pronounced peaks in magnitude in the recompression region and in the developing wake. The interface convolution increases monotonically with downstream distance in both the side- and end-view orientations.

Introduction

THE nature and structure of turbulence in compressible shear flows are still not fully understood. A better understanding of this turbulence is critical to efforts to control supersonic vehicles and projectiles, lower their base drag, or change their radar signature. Past efforts have determined the mean size, shape, and eccentricity of the large-scale turbulent structures present in planar[1] and axisymmetric[2] supersonic base flows and in highly compressible mixing layers[3–5] using Mie scattering from condensed ethanol droplets as the primary diagnostic. These studies give useful information about the mean turbulent structures that are on the scale of the local shear layer thickness, but the technique employed to analyze the images does not provide any information about larger scale motions, such as shear layer flapping or the effect that the structures have on the convolution, that is, tortuousness or degree of folding and twisting, of the shear layer interface. The present study addresses these issues.

Shear Layer Steadiness and Flapping Motions

Most of the documented research in flapping is for low Reynolds number planar shear layers and jets.[6,7] For a planar nozzle geometry, the apparent flapping motions are derived from asymmetric staggering of the large vortices that form from the rollup of Kelvin–Helmholtz-type instabilities, on either side of the jet. A classic example of flapping motion is shown in the von Kármán vortex street formed by shedding in the wake of a cylinder in crossflow.

The high level of compressibility ($M_\infty = 2.46$ and $M_c = 0.49$–1.4; see Table 1) and large Reynolds number (52×10^6 m^{-1}) dictate that motions of the type just described for incompressible, low Reynolds number flows are not present in the current supersonic, separated flow.[8] In compressible, axisymmetric flows, flapping motions are thought to be generated by the propagation of helical disturbances,[8,9] which must be pumped by feedback from downstream disturbances such as obstacles[10] or shock structures.[9] Ponton and Seiner[8] showed that the flapping motions of an axisymmetric jet with an exit Mach number of 1.3 are generated by double-helix disturbances developed from instabilities generated at the nozzle lip via feedback from downstream shock structures. Similar phenomena can occur within the recirculation region in the present separated flow.

Variability in the shear layer position can also be generated by pressure fluctuations in the freestream. Asymmetric circumferential pressure fluctuations can contribute to motion of the centroid of the enclosed wake core area (in the end view), whereas circumferentially symmetric pressure fluctuations can contribute to fluctuations in the magnitude of the recirculation and wake core areas and variability in the location of the reattachment point.

Smith[11] reported unsteady shear layer motions with a magnitude of approximately one-third of the local shear layer thickness in a planar, supersonic, reattaching base flow. Although his geometry was planar rather than axisymmetric, as in the current flow, the mechanisms that cause this unsteadiness (feedback through the recirculating flow region, pressure fluctuations in the freestream) can produce similar results. Both symmetric and asymmetric motions can occur, leading to either area-magnitude fluctuations or shear layer flapping, respectively.

Interface Convolution

Two sources were found that attempted to describe qualitatively the effect of compressibility on the convolution of the interface between fluids in a planar shear layer. Clemens and Mungal[4] claim that the convolution of the interface, when visualized from the end-view orientation, increases with convective Mach number, whereas Island et al.[12] claim that the overall interface appears smoother for higher convective Mach numbers. These statements do not necessarily conflict because these studies also show that, as convective Mach number increases, the organization of the large-scale turbulent structures changes from a spanwise to a streamwise orientation and the coherence of the structures decreases. Therefore, in the end-view plane, the degree of interface convolution can increase while the overall interface convolution decreases at higher levels of M_c. Clearly, quantitative results are necessary to elucidate and verify observations such as these.

Very few studies have been performed to determine directly the convolution of the interface of compressible shear layers, even though this is an important indication of the mixing potential between two streams. Two common practices that have been cited in the literature to determine interface convolution are determination of the fractal dimension[13,14] and direct calculation of the length of the interface.[15] The fractal dimension classification asserts that the mixing interface is composed of degenerate patterns that repeat themselves throughout all scales of the flow. These studies show that mixing interfaces most commonly have a fractal dimension between 2.2 and 2.7 (Refs. 13 and 14). The interpretation and usefulness of fractal results in fluid mechanics applications are not particularly clear, and the method is not widely used. The interface length technique is more straightforward. This method postulates that there is a surface (or line in a two-dimensional image) that corresponds with a

Received 20 June 1999; revision received 9 February 2000; accepted for publication 16 February 2000. Copyright © 2000 by the American Institute of Aeronautics and Astronautics, Inc. All rights reserved.

*Graduate Research Assistant, Department of Mechanical and Industrial Engineering. Student Member AIAA.
†W. Grafton and Lillian B. Wilkins Professor, Department of Mechanical and Industrial Engineering. Associate Fellow AIAA.

Table 1 Coordinates and flow parameters at imaging positions

Imaging position	Location	Distance from base corner, mm	Convective Mach number M_c	Mie scattering shear layer thickness δ_{Mie}, mm	LDV velocity shear layer thickness δ_{Vel}, mm	Mie scattering shear layer angle, deg	End-view recirculation/wake core area A_{mean}, mm^2
A	Shear layer	18.4[a]	1.23	2.47	5.9	12.7	2610
B	Shear layer	36.8[a]	1.40	3.67	9.3	14.0	2040
C	Recompression	72.4[a]	1.24	4.42	12.5	9.3	1016
D	Reattachment	84.1[b]	1.09	4.98	13.6[c]	——	456
E	Near wake	135[b]	0.49	13.69	——	——	754

[a]Measured along shear layer. [b]Measured along centerline. [c]Estimated.

minimum potential for mixing in any geometry.[15] The actual mixing interface length can then be ratioed with this minimum mixing interface length to indicate the increased potential for mixing caused by the increased interfacial area available.

Because of its relative simplicity, the length–ratio technique is employed in this study. A paper, by Glawe et al.[15] employed this method to determine the mixing potential of a streamwise jet injected from the base of a strut into a supersonic freestream. They found that a range of shape factors, from approximately 2 to 4, could be attained by varying the cross-sectional shape and exit velocity of the jet.

Equipment and Diagnostics

The data presented in this paper have been gathered from experiments performed in the Gas Dynamics Laboratory at the University of Illinois at Urbana–Champaign. The axisymmetric base flow facility generates a Mach 2.46 flow about a 63.5-mm-diam cylindrical afterbody/blunt base. The base flow tunnel is characterized by a relatively low freestream turbulence intensity (<1%), a turbulent boundary-layer thickness at the trailing edge of the afterbody of 3.2 mm, and a unit Reynolds number of $Re = 52 \times 10^6$ m^{-1}, as cited in the laser Doppler velocimetry (LDV) data of Herrin and Dutton.[16]

Flow visualization of the interface between the freestream and recirculation/wake core regions have been accomplished in the current experiments by implementing the same Mie scattering technique as Smith and Dutton[1] and Bourdon and Dutton.[2] Ethanol vapor was seeded into the supply airstream. As it is rapidly accelerated in the converging–diverging nozzle, the ethanol vapor condensed into a fine mist of approximately 0.05-μm-diam droplets,[11] which are easily small enough to follow the large turbulent structures.[17] The condensation characteristics of ethanol dictate that, in our facility, the ethanol will condense at all flow speeds higher than approximately sonic conditions. Thin slices of this ethanol fog were illuminated via a 200-μm-thick laser sheet formed from a Nd:YAG laser with a nominal pulse energy of 450 mJ/pulse and at a pulse frequency of 10 Hz (Fig. 1). A high-resolution, 14-bit unintensified charge-coupled device (CCD) camera was used to record the scattered light. End-view images were obtained by rotating the cylindrical mirrors in the optics train and positioning the camera off-axis. A geometric transformation was then applied to the images to obtain a true end view. Many more details concerning the flow facility and visualization method may be found in Refs. 1 and 2.

General Flowfield Characteristics

Figure 2 is a global Mie scattering image of the flowfield in question. This flow is driven in large part by the base-freestream pressure and velocity mismatches that result from the sudden termination of the afterbody and the attendant flow separation. Expansion waves emanate from the base corner, and a free shear layer forms as a result of the pressure and velocity mismatches, respectively. Because the intensity of the Mie scattered light is proportional to the number density of the ethanol droplets, which is reduced across the expansion, the expansion appears as a dark region emanating from the base corner. As the shear layer approaches the axis of symmetry, the mean flow must turn parallel to the axis. An adverse pressure gradient and, thus, recompression waves in the supersonic freestream develop due to this turn along the axis of symmetry. These recompression waves are indicated in Fig. 1 by the discontinuous bright

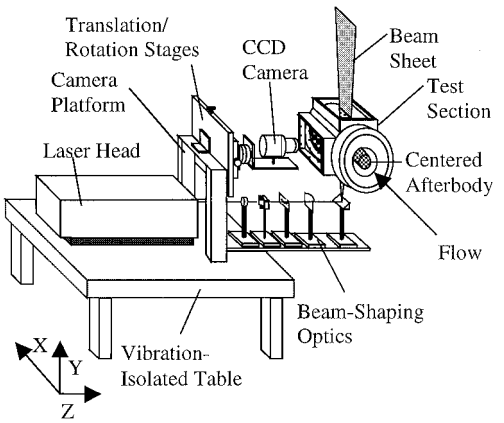

Fig. 1 Mie scattering image acquisition system.

bands near the right center of the image. Lower velocity fluid on the inner edge of the shear layer does not possess sufficient kinetic energy to negotiate the recompression process and is turned back toward the base, forming a large recirculation region. Because the air in this region is at relatively low velocity, and is therefore warm, condensed ethanol is not present, and light scattering by the laser sheet does not occur. A point, X_r in Fig. 2, exists where the mean velocity along the axis is zero and is termed the reattachment point.[16] This point delineates the recirculation region immediately behind the base from the trailing-wake region.

Bourdon and Dutton[2] have recently completed a detailed study of the size, shape, and orientation of the large-scale turbulent structures present in this flow. This study examined five specific regions in which various features of the mean flowfield are expected to have the greatest influence. These locations are shown in Fig. 2. Positions A and B are in the postseparation shear layer, before the strong influence of the adverse pressure gradient. This strong adverse pressure gradient is in full effect by position C, and position D is located at the mean reattachment point. Position E is located in the trailing wake that develops downstream of the reattachment point.

Figures 3 and 4 show instantaneous side- and end-view images, respectively, from imaging locations B–E. Images from position A have been excluded for the sake of brevity; qualitatively, they are very similar to those at position B. The side-view turbulent structures (Fig. 3) appear to be dramatically enhanced in size by the adverse pressure gradient (position C). They also appear much more organized in the developing wake (position E), partially because of the lower convective Mach number in this region (0.49 vs about 1.3 farther upstream; see Table 1). The turbulent structures generally appear to be more regularly spaced in the end views (Fig. 4) than in the side views. There is a relatively constant number of structures in each frame at each end-view imaging position, but this number decreases with downstream distance. These end-view structures also occupy a larger percentage of the core fluid area with increasing downstream position.

Results and Discussion

The current study examines the same five imaging positions as the earlier Bourdon and Dutton[2] study (Fig. 2) and quantifies the effects of flapping and mixing interface convolution in these regions.

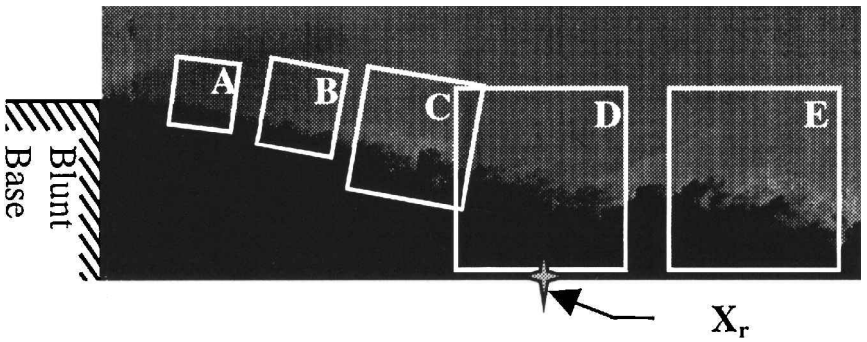

Fig. 2 Instantaneous global composite image of near-wake flowfield and illustration of fields of view used.

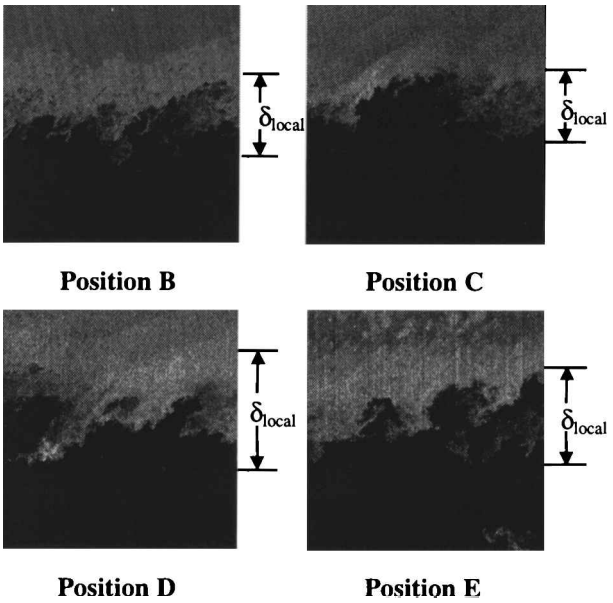

Fig. 3 Instantaneous side-view images typical of those gathered at positions B–E.

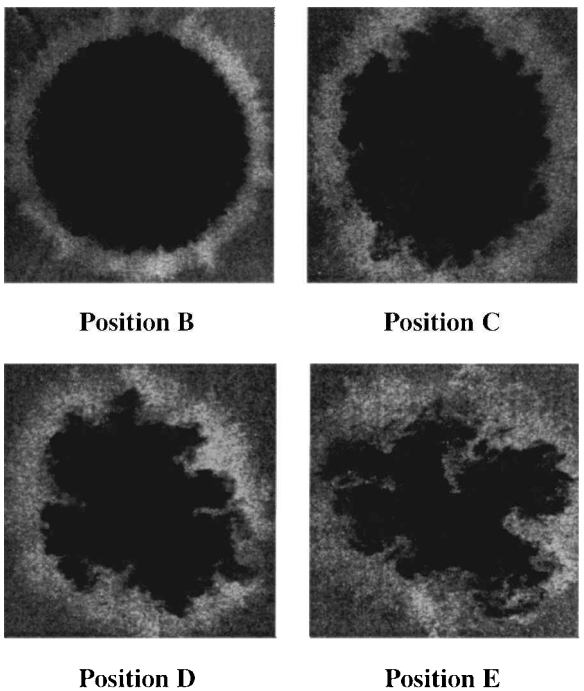

Fig. 4 Instantaneous end-view images typical of those gathered at positions B–E.

Reference 2 presented only ensemble-averaged results for the mean large structure size, angular orientation, and eccentricity and did not consider flapping or convolution of the shear layer, as discussed here. The techniques used in the current work aid in interpreting the spatial correlation analysis and LDV measurements previously performed in this flowfield and provide a vital link between the overall nature of the shear layer and the large-scale turbulent structures that dominate its development. The five imaging positions shown in Fig. 2 were chosen to characterize best the behavior of the four major regions of interest (postseparation shear layer, recompression region, reattachment region, and developing wake) along the path of the reattaching shear layer. The locations of and other pertinent information about the five imaging positions are presented in Table 1. The convective Mach number and velocity shear layer thicknesses presented in Table 1 were estimated from the LDV data of Herrin and Dutton.[16] Approximately 500 images were acquired at each imaging position and in each view. Ensembles of this size were found by Smith[11] to produce converged mean and rms images.

Note that the Mie scattering thicknesses are approximately 40% of the velocity thicknesses reported by Herrin and Dutton[16] in the same flowfield and correspond to approximately the 90–50% mean velocity locations, or roughly the outer-half of the shear layer. This difference results because the intensity gradient visualized with the Mie scattering technique is generated entirely by low-temperature, that is high-speed, fluid, which lies in the outer-half of the shear layer. Thus, when considering these results, one must keep in mind that the structures seen in the images and the statistics presented are for effects seen in this outer region.

Shear Layer Large-Scale Motion Analysis

The large-scale motion (or flapping) of the shear layer is an important factor in determining the turbulence mechanisms that act on the shear layer and in interpreting other experimental results. The motion of the shear layer can indicate the presence of global instabilities, for example, axisymmetric or helical motion, that may not be detected by spatial covariance analysis.[1,2,5] Also, if a shear layer is actively flapping, it can artificially increase LDV turbulence statistics and smear image covariance analyses. For these reasons, a technique has been developed to characterize the nature of the shear layer large-scale motion.

Side View

In the side-view orientation, we assume that the large-scale motion occurs normal to the mean local shear layer isointensity lines. With this assumption made, the bulk shear layer motion can be characterized by obtaining a spatially averaged shear layer position from each instantaneous image. Such averages were used to limit the effect that the passage of a single large-scale structure would have on the perceived flapping measurement. This average is determined by collapsing the image in the streamwise direction to obtain the transverse intensity profile. The shear layer position is then determined by locating the intensity level that is 20% of the maximum value, which approximates the inner edge of the shear layer. The instantaneous intensity profile across the shear layer thus obtained is relatively insensitive to skewness in the shear layer's position, and so this technique is not ideal for detecting motion that is not normal

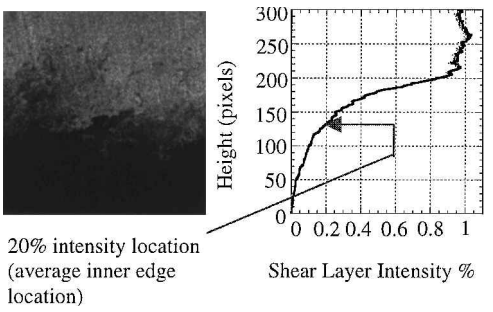

Fig. 5 Spatially averaged instantaneous intensity profile from a typical side-view image.

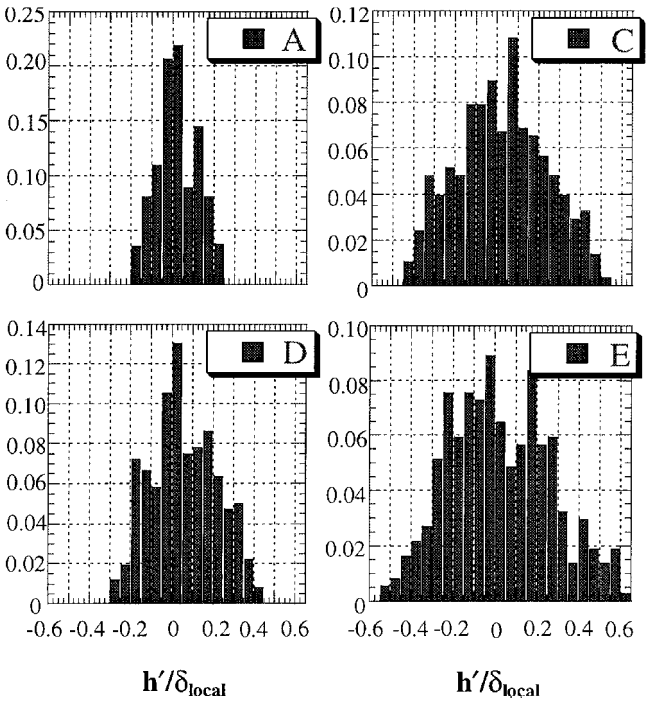

Fig. 6 Histograms of transverse shear layer motion at positions A, C, D, and E gathered from side-view images.

to the mean image isointensity lines. See Fig. 5 for an example of a streamwise-averaged intensity profile from an instantaneous image.

Figure 6 shows probability density functions (PDFs) of the shear layer displacement from its mean location normalized by the local shear layer thickness h'/δ_{local} as seen in the side views at positions A and C–E. The results at the upstream locations, positions A, B (not shown), and C, display a nominally Gaussian shape with a pronounced central peak. The near-Gaussian PDF shape at these locations indicates the presence of a single preferred shear layer position. In the reattachment region, position D, the distribution of instantaneous displacement values is more uniform across the span of the PDF, losing the Gaussian shape observed at the locations upstream of reattachment. This demonstrates that there is no clearly dominant preferred shear layer position in the region surrounding the mean reattachment point. Incoherent flapping motions in this region are yet further indications of the decrease in turbulence structure organization that accompanies the reattachment process.[1,18] The displacement histogram displays a bimodal or possibly even trimodal shape at position E in the trailing wake, and the PDF is even wider than at the upstream locations. The lower convective Mach number at this wake location ($M_c = 0.49$) allows for a higher degree of turbulence organization and better defined peaks in the shear layer displacement histogram than at position D. An illustration of the shear layer displacement at position E is shown in Fig. 7. The images in Fig. 7 are representative of typical images from the two displacement peaks of the PDF near $h'/\delta_{local} = \pm 0.2$. Note that there is no obvious difference in the turbulent structure between these frames. This

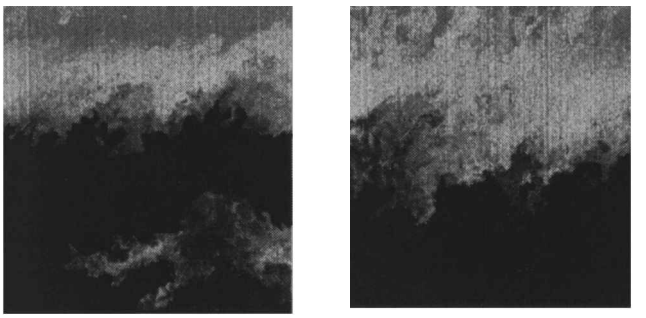

Fig. 7 Side-view shear layer displacement at position E.

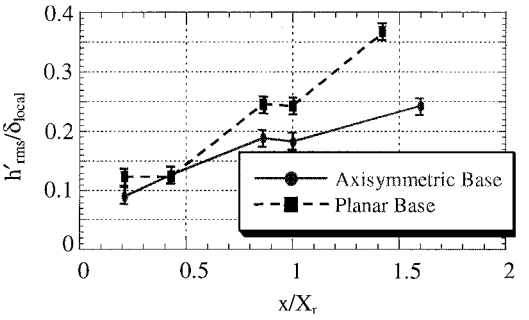

Fig. 8 Side-view rms displacement of freestream/shear layer boundary from mean position normalised by local shear layer thickness for positions A–E.

motion could be due, then, to differences in the amount of fluid escaping from the recirculation region at each instant imaged.

The rms displacement of the side-view motion at each imaging position is plotted in Fig. 8, for both the present axisymmetric geometry and the planar geometry studied by Smith and Dutton.[1] This normalized representation (by δ_{local}) is most appropriate for judging the local significance of the flapping motions and their effects on the local turbulence structure. Therefore, this view of the shear layer motion provides a more relevant vantage point when determining the effect that these motions will have on turbulence quantities that have been gathered by LDV or other pointwise velocity measurement techniques in this flow, for example, interpretation of flapping unsteadiness as turbulence.

As shown in Fig. 8, the rms fluctuations of the shear layer position are up to 25% of the local thickness in the axisymmetric base flow. The planar shear layer results are consistently larger than the axisymmetric results, except at position B where they are equal. This suggests that the geometrical constraints placed on the axisymmetric shear layer as it approaches the axis of symmetry tend to dampen large-scale motions.

In both geometries, the normalized rms displacement generally increases at successive axial locations, until the reattachment point, position D. The reduced flapping (in relation to δ_{local}) at this location is consistent with the symmetry condition that must be enforced (in a time-averaged sense) as the shear layer approaches the axis and reattaches onto itself. This reduction is slightly weaker in the planar case because the reattachment process in that case occurs along a line, whereas in the axisymmetric case, it occurs at a point. This streamline convergence for the axisymmetric geometry has been shown[18] to stabilize the turbulence field. The increased rms displacement at position E can be attributed more to the presence of multiple preferred positions (Fig. 6) than to a pure broadening of the PDF as noted at the initial imaging locations, positions A–C. Considering that the Mie scattering thickness δ_{local} is less than half of the velocity thickness at each location (Table 1), these rms flapping motions are rather small, all being less than 15% of the local velocity thickness.

Because normalization by the local shear layer thickness was used in Fig. 8, this plot displays a different trend than that viewed when

h'_{rms} is nondimensionalized by a constant length scale, such as the base radius. This interpretation indicates that the shear layer flapping fluctuations are very small in a dimensional sense (about 1 mm or 3% of the base radius) before reattachment, and they increase by a factor of over four at the imaging position in the developing wake. This agrees well with what was seen by direct observation while experiments were performed. The flapping motions, from a global or dimensional perspective, are negligible through the reattachment region. Only in the wake development region are the flapping motions significant compared to the base radius.

End View

In many respects, it is much more natural to view the effects of flapping and pulsing motions in the end view than in the side view. In this view, a global perspective of the shear layer is seen a given distance downstream of the base. Because the end view of the axisymmetric shear layer is a nominally circular, closed curve, the bulk motion is not derived using the same technique as was used for the side view. The motion viewed as flapping in the side view can be separated into two distinct types of motion in the end view: pulsing (or expansion/contraction) of the core region and displacement of the centroid of the shear layer. Therefore, a technique has been developed to isolate these two effects.

The nominally circular shape of the end-view shear layer can be exploited to develop intensity profiles across the shear layer similar to those from the side view. A circumferentially averaged radial intensity profile about the instantaneous core centroid is generated similar to the linearly averaged profiles in the side view. Core fluid is defined for this purpose as any pixel that has an intensity of less than 20% of the average intensity in the freestream, and the centroid is defined as the area center of all core fluid pixels. The variation in area occupied by the core fluid indicates the magnitude of pulsing motions, whereas the motion of the core fluid centroid characterizes the displacement of the shear layer from its nominal position.

Scatter plots of the instantaneous core-region centroid positions, normalized by the local shear layer thickness, are shown for the end views at imaging locations B–E in Fig. 9. The discretized appearance of the instantaneous centroid positions at position B is an artifact of the resolution of the CCD camera. The diameter of the core fluid region at positions A and B is approximately 400 pixels, whereas the instantaneous centroid position varies at these locations by only approximately 5 pixels in any direction.

The magnitude of the centroid-position variations at imaging locations A (not shown) and B in the shear layer are similar, with roughly random variations in all four quadrants, at a maximum

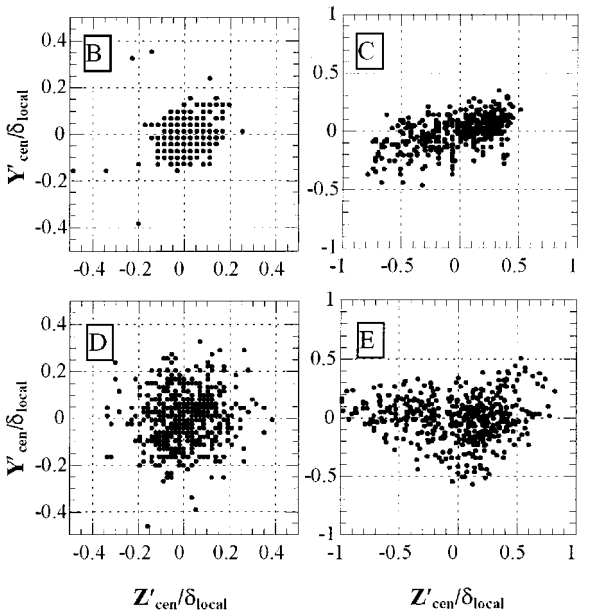

Fig. 9 Maps of instantaneous recirculation/wake core centroid position at imaging locations B–E, end view; *Y* and *Z* are vertical and horizontal directions, perpendicular to the downstream direction *X*.

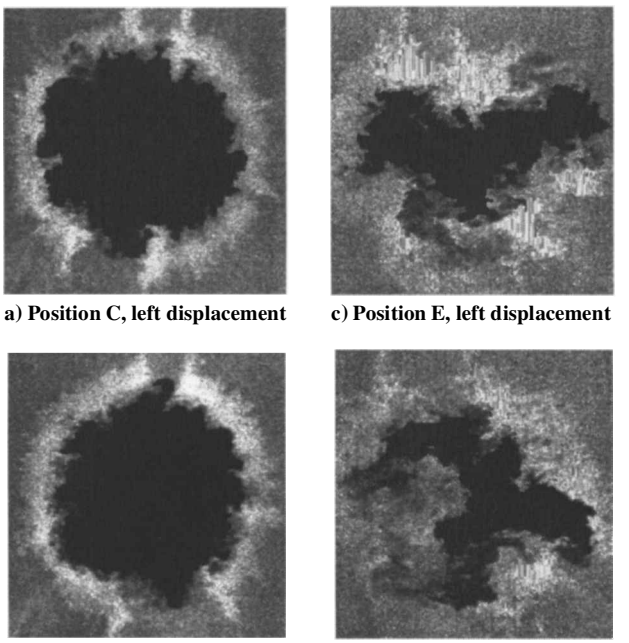

Fig. 10 Instantaneous images demonstrating centroid motion along *Z* axis.

of about 0.2 shear layer thicknesses about the mean location. The centroid-position variations at the mean reattachment point, position D, are also similar to those at positions A and B in distribution, but with a slightly larger magnitude (Fig. 9). Positions C and E in the adverse pressure gradient and developing wake regions, on the other hand, exhibit a horizontal, sloshing type of motion, predominantly along the *Z* axis. The magnitudes of the centroid motions at these two locations are also much larger than at the other stations.

The sloshing motions exhibited at positions C and E require further examination. Instantaneous images that illustrate this motion of the centroid along the *Z* axis are shown in Fig. 10. It is clear after examining these images that the large, mostly horizontal centroid displacements at these locations are caused by an asymmetry in the distribution of the largest turbulent structures about the shear layer circumference. This is evidence that the apparent flapping or unsteadiness visualized in the end-view orientation in this flow is caused predominantly by the passage of these very large structures, which is similar to the results found in incompressible, axisymmetric jets.[7]

This large-scale structure asymmetry could possibly be due to a double-helix instability that alters the organization of the large structures and is somehow anchored in these regions to allow only horizontal motions. These centroid-position results could also be caused by slight misalignment of the sting/afterbody in the annular converging–diverging nozzle of the flow facility. Further analysis has indicated that this latter explanation is unlikely, however. Rotating the afterbody has little or no effect on the axis of the sloshing motions, and oil-streak visualizations on the base do not indicate any flow asymmetry. However, if either misalignment or helical modes are responsible for this asymmetry, it is difficult to understand why it is only present at positions C and E, and not at A, B, and D, and why it occurs mostly along a single axis. Perhaps the lack of similar motions at the early imaging locations, positions A and B in the postseparation shear layer, can be attributed to the constraint placed on the shear layer motion by its proximity to the base and the lack of strong pressure gradients in the freestream. It is also possible that there is asymmetry in the turbulent structure organization at these locations, but the scale of the structures in relation to the recirculation region is so small that the effects are below the resolution limit of the CCD camera. The effects of lateral streamline convergence and axisymmetric confinement at the mean reattachment point,[2,18] position D, may act to randomize the positioning of the large-scale structures, or turbulent structure amalgamation may be occurring in a way that causes a more symmetric distribution of the structures

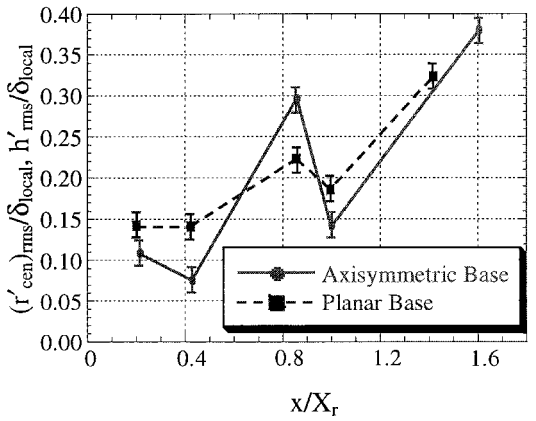

Fig. 11 End-view rms displacement of recirculation region/wake core centroid from mean position, normalized by local shear layer thickness.

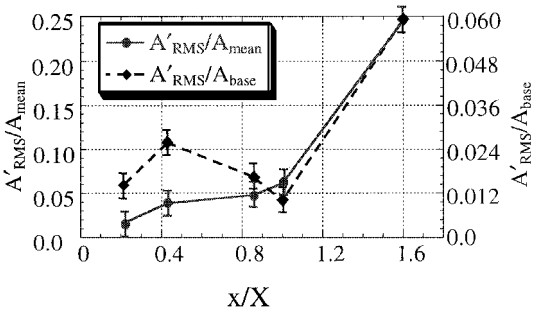

Fig. 12 End-view rms variation of enclosed recirculation/wake core area normalized by the local mean area and base area at positions A–E.

about the shear layer periphery in this region. Position C, with its characteristically large adverse pressure gradient and recompression waves, and position E, with its lower convective Mach number and reaccelerating wake core fluid, may be most susceptible to large-scale motion of the centroid. Further work is needed to determine the root cause of this curious behavior.

The rms radial displacement of the end-view centroid from its mean location, scaled by the local shear layer thickness, at all five imaging locations is plotted in Fig. 11. The rms end-view displacement (h'_{rms}/δ_{local}) in Smith and Dutton's planar reattaching supersonic flow[1] is plotted alongside the axisymmetric results. Although the two measurements are not precisely of the same motion, that is, the planar measurements do not differentiate pulsing and translating motions, the similarity between the results at the various positions is clear. This suggests that the mechanisms responsible for these motions must be quite similar in the two geometries. The sloshing motions at positions C and E for the axisymmetric case cause large peaks with magnitudes in the range of 30–40% of the local shear layer thickness, whereas positions A, B, and D all have magnitudes of less than 15% of the local thickness. The end-view motions for the planar case are generally larger than those for the axisymmetric base, except in the adverse pressure gradient region, position C. Figure 11 is valuable in determining the effect that these motions may have on pointwise velocity statistics; clearly these effects are largest at positions C and E in the adverse pressure gradient and wake development regions.

Just as in the side view, the end-view flapping motions appear quite different when viewed from a global, dimensional perspective. Aside from the motion at position E in the trailing wake, the centroid position varies by less than 4% of the axisymmetric base radius. At position E, the rms value of the centroid-position fluctuation increases to approximately 16% of the base radius.

Figure 12 shows the rms fluctuation of the normalized recirculation/wake core fluid area for the five imaging locations of this study normalized by both the local mean area and the area of the base. The rms variation is small, less than 6% of the local A_{mean}, at positions A–D, and is quite large, just under 25% of A_{mean}, at position E in the near wake. Recall, however, that the percentage of the instantaneous area of the wake core at position E that is composed of large turbulent structures is much higher than at previous locations, and the wake core region is of a smaller absolute area compared to locations A–C (Fig. 4 and Table 1). Therefore, the much larger percentage area variation at this location is a result of the increasing contribution of the largest turbulent structures to the relatively small wake core area. Note in Fig. 12 the trend to lower rate of increase in the area variation between positions B and C (A_{mean} normalization) as compared to between the other locations. Therefore, the adverse pressure gradient (which is present at C but not at A and B) acts to reduce the rate at which the area variations grow as the flow proceeds downstream. The growth of area fluctuations does increase slightly between positions C and D as compared to between locations B and C. This enhanced area variation in the neighborhood of reattachment suggests that the instantaneous reattachment point translates upstream and downstream, as expected.

Discerning the absolute magnitude of these area fluctuations is difficult when they are scaled by the local enclosed area A_{mean}. These area fluctuations can be critical in judging the relative strengths of the expansion/contraction motions as they progress downstream. Therefore, the area variations are also plotted in Fig. 12 as normalized by the (constant) base area. One interesting feature illustrated by this normalization is the substantial increase in dimensional area fluctuations at position B, as compared to A, and the steady decrease through the recompression and reattachment processes. At the upstream positions A and B, axisymmetric effects are negligible because the shear layer is far from the axis. The recompression and reattachment processes, on the other hand, are a direct result of the shear layer approaching the axis of symmetry. Note also that the rate of decrease in the magnitude of area fluctuations increases as the shear layer moves closer to the symmetry axis at reattachment position D. At position E in the trailing wake, the area fluctuations are greatly enhanced, even though the wake core/freestream interface is very near the axis. Thus, it is the impingement of the shear layer on the symmetry axis at reattachment that inhibits area-based fluctuations in this region. Note, however, that the rms area fluctuations at all imaging locations are relatively small in a dimensional sense, being less than 6% of the base area in all cases.

Mixing Interface Convolution Analysis

Valuable information is gained from examining the area available for mixing at a given location. If the interface between the freestream and recirculating fluid is defined, and its length measured and compared with a limiting case, the mixing potential of that region can be examined. The limiting case is defined here as the boundary shape for a given geometry for which minimum mixing would occur. For example, in either a side view or end view of a planar shear layer, the limiting boundary shape would be a line, whereas in the end view of a round jet, a circle would be the limiting case.

An arbitrary contour, corresponding to 15% of the maximum averaged intensity in the shear layer of a given image, was chosen to represent the actual mixing interface in this convolution study. Figure 13 presents a sample end-view image from position E, the interface between the freestream and core fluids, and the area enclosed within this interface. Testing of this technique shows that it is fairly robust and insensitive to the intensity level chosen to mark the interface, within the range of 5–15% of the peak mean intensity value in each image.

Note that the image resolution of these experiments is not adequate to resolve small-scale mixing. However, the goal of this study is to examine the effects of the large-scale structures on the development of the shear layer rather than to quantify mixing characteristics at the smallest scales. Therefore, a series of filters was applied to remove smaller structures and irregularities from the interface. These filters set an effective lower limit on the degree of curvature or irregularity that registers at the boundary that separates the freestream and core fluids. The limit can be changed to reflect the differences in scale from one image set to the next to ensure that consistent boundary resolution is applied throughout the study. In the present investigation, the mean shear layer occupies approximately one-third of the image frame at each location, so that the filtering parameters were held constant throughout the analysis.

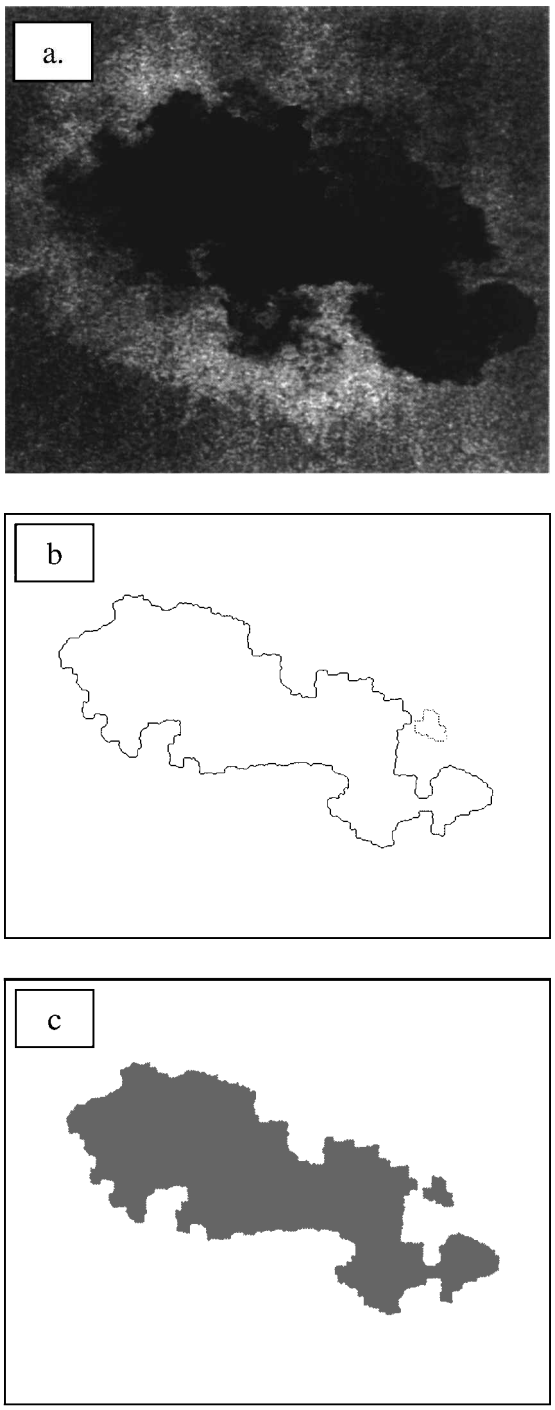

Fig. 13 Shape factor 2.19: a) sample end-view image, b) border of sample image, and c) enclosed area.

Examining the shape factors (defined as the actual to minimum interface length) of large ensembles of images at a given location in the flowfield aids in understanding the nature of the turbulence in that region. The nature of the frequency histogram, that is, the number and strength of peaks, and the mean and standard deviation of the histogram yield valuable information about the organization of the large-scale structures. The height and breadth of the histogram peaks indicate how consistent and repeatable the large-scale structure pattern is. Also, when this analysis is viewed in conjunction with information about the mean size, shape, and orientation of the large-scale structures,[2] the relative abundance and variety of turbulent structures at a given location can be conjectured.

Side View

In the side-view orientation, the mean shear layer is essentially a linear interface. In such a geometry, minimal mixing will, thus,

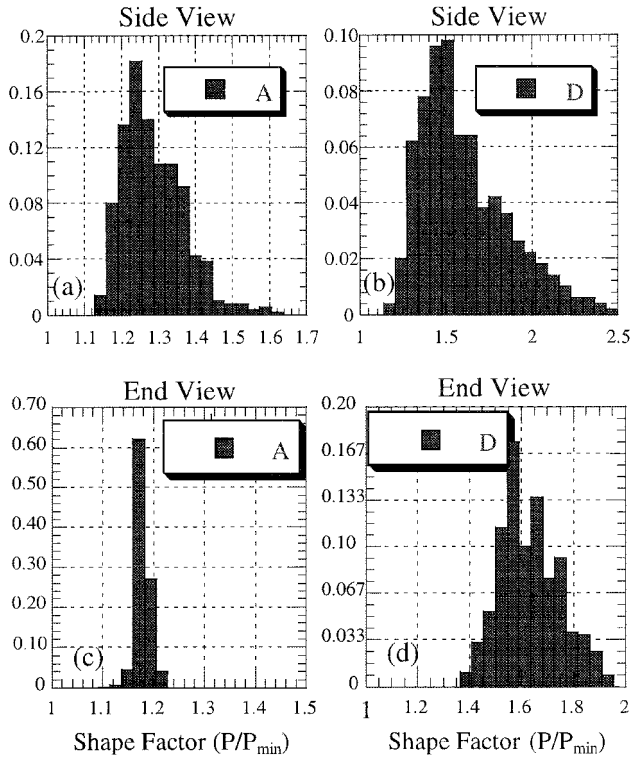

Fig. 14 Histograms of interface shape factors: a) position A side view, b) position D side view, c) position A end-view, and d) position D end view.

occur for a straight-line interface. Therefore, the proper shape factor in this view is defined as the instantaneous shear layer length ratioed with the local mean (linear) shear layer length. The more the instantaneous interface deviates from linearity, the higher the value of the shape factor and the greater the potential for mixing.

Figures 14a and 14b present histograms of the instantaneous side-view shape factors for positions A and D. These histograms are representative of the side-view shape factor histograms at all five imaging locations. Note that the most probable shape factor and the shape factor variability (PDF width) shown in the side-view histograms generally increase at successive locations. Also, unlike the histograms presented in the last section for shear layer motion, these histograms suggest a gamma distribution of shape factor values. Because the mean values at all imaging positions are relatively close to unity, the lower range limit, and the rms deviation is relatively large, this is intuitively logical. A process with these characteristics naturally fits a distribution such as the gamma distribution, which is skewed toward lower values. This distribution shape remains relatively consistent through all five imaging locations.

The mean shape factor increases monotonically with increased downstream distance in the side view for both the axisymmetric and planar geometries (Fig. 15a). There is a close similarity between the results for the two geometries. The absolute value and rate of increase of the shape factor in the side-view orientation are slightly larger for the planar geometry, but the other major trends are virtually identical. This suggests that the degree of convolution of the shear layer is relatively insensitive to parameters that differ between the two geometries in each measurement region, such as the location of the peak Reynolds stress or the effect of lateral streamline convergence.[18]

The shape factor increases monotonically and at a relatively constant rate throughout the separated flow region, positions A–D, for the axisymmetric case. Therefore, the adverse pressure gradient and reattachment process have little or no effect on the side-view convolution growth, despite the rapid growth in mean structure size in this region.[1,2] Smith[11] showed that, for a planar reattaching base flow, the large-structure convection velocity decreases dramatically in the adverse pressure gradient region. Therefore, it is reasonable to speculate that the mean structure growth in this region is caused

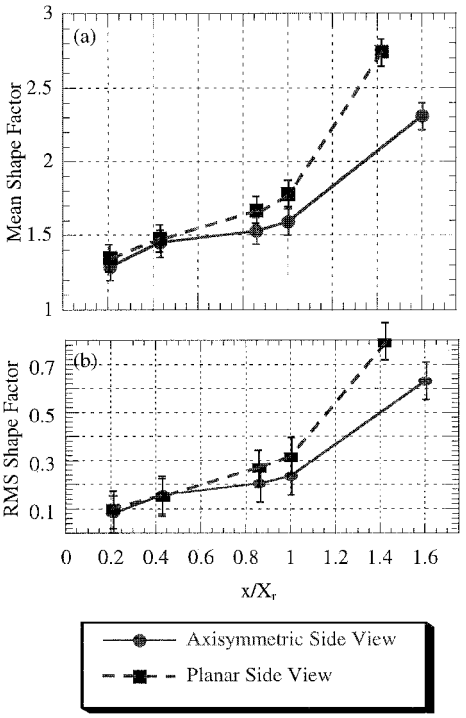

Fig. 15 Side-view shape factors at positions A–E for both axisymmetric and planar[1] geometries: a) mean and b) rms.

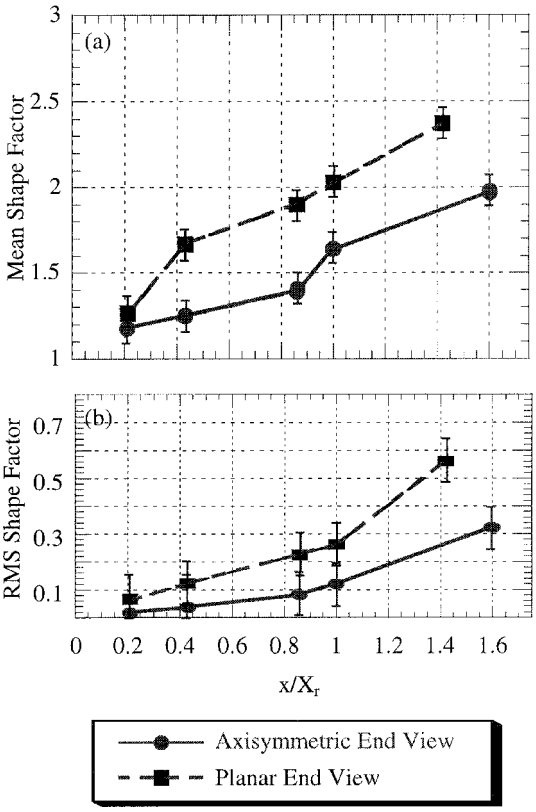

Fig. 16 End-view shape factors at positions A–E for both axisymmetric and planar[1] geometries: a) mean and b) rms.

by amalgamation of the large turbulent structures formed upstream and that enhancement of mixing (and increased shape factor) is not large through this region. This amalgamation process may occur as Oh and Loth[19] propose for compressible shear layers, that is, that the large-scale structures simply slap into one another and merge, without any significant transverse deflection or rotation about each other as occur in incompressible pairing processes.[20,21] This type of merging process results because, as the convective Mach number increases, communication paths between large structures are suppressed, that is, pressure waves cannot travel upstream fast enough to communicate the preceding structure's presence before a collision occurs between two structures.[19] A merging process of this type would also account for the significant decrease in mean structure angle that accompanies the rapid increase in structure size in the adverse pressure gradient region.[1,2]

In the developing wake (between positions D and E) for both geometries, the rate of increase of the shape factor is larger than in the initial portions of the postseparation shear layer that forms immediately downstream of the base, that is, between positions A–D. Therefore, the rate of increase of the shear layer convolution, and the size and organization of the large-scale structures, is most likely influenced by either changes in the velocity ratio, the reduced convective Mach number, or the enhanced growth of the wake thickness when compared to the growth of the shear layer prior to reattachment (Table 1).

The rms variation of the side-view shape factor increases almost linearly with increased downstream position between positions A and D for both planar and axisymmetric flows (Fig. 15b). This shows that the variability of the interface convolution caused by the turbulent structures increases steadily in the streamwise direction regardless of the flow mechanisms acting on the structures. Position E is the exception to the pattern; the rate of increase of the rms shape factor between D and E is higher than between the initial locations. This latter result could be due to the dominance of very large structures at position E. Variations in the number of these largest structures that are captured in a given image could lead to large variations in the instantaneous shape factor at this location and, thus, to a large rms value.

End View

In the end-view orientation for the axisymmetric case, the shear layer forms a closed contour, for which minimum mixing will occur when the shear layer is circular. The shape factor is then defined as the actual instantaneous interface perimeter ratioed with the minimum (circular) perimeter enclosing the equivalent area. The instantaneous end-view shape factor histograms are much less skewed toward low values than those obtained in the side-view orientation and appear approximately Gaussian; see Figs. 14c and 14d for the end-view shape factor histograms at positions A and D. The variation of the instantaneous shape factor, that is, histogram breadth, is also smaller at each station in the end views than in the side views, especially at the initial imaging locations. This suggests a higher degree of consistency of the structures visualized in the end view than in the side view, which results from the relatively constant number of large-scale structures present in each frame for each imaging position of the end views (Fig. 4).

The mean shape factor values for all five end-view imaging positions are shown in Fig. 16a for both the axisymmetric and planar bases. The shape factor is seen to increase monotonically with increasing downstream distance from separation for both geometries. Consistently larger shape factor values are seen at each position and in both the side view and in the end view for the planar case. Bourdon and Dutton[2] have shown that the geometry of the separated flow region has little effect on the growth of the large-scale turbulent structures outside of the reattachment region. Therefore, because the mean structures are similar for the two geometries, this larger shape factor value in the planar geometry must be related to the organization or mean spacing of the structures. Figure 16 also shows that the adverse pressure gradient (between positions B and C) has little or no effect on increasing the rate of shear layer convolution as the flow progresses downstream in the axisymmetric geometry. Therefore, if the proposed streamwise amalgamation of the turbulent structures occurs in this region, it has no visible effect on the rate of increase of the end-view shape factor.

The axisymmetric reattachment process (position D) clearly enhances the convolution of the enclosed fluid boundary in the end view. This result is to be expected because of the highly three-dimensional nature of the reattachment process. The three-dimensional nature is also evident because the side- and end-view mean shape factor values are approximately equal at the

reattachment point. The rapidly decreasing number, but increasing size, of structures present due to structure amalgamation and shrinking core fluid area are also key features of the flow in this region, and they contribute to the enhanced shape factor values at position D. These latter features are clearly seen in the example images presented in Fig. 4. Because the planar reattachment process does not involve the circumferential confinement effects seen in the axisymmetric reattachment process, little or no change in the shape factor growth rate at position D in the end view is observed.

After the reattachment process is complete, the axisymmetric confinement effects that cause the increased shape factor growth rate are relaxed, and the rate returns to the prereattachment region values. The end-view shape factor continues to increase in the trailing wake, position E, approaching a value of 2 for the axisymmetric case and 2.4 for the planar case. Note that the end-view shape factor values recorded in the current study span the same range observed by Glawe et al.[15] in their study of parallel injection from the base of a strut into a supersonic coflow.

The rms shape factor evolution (Fig. 16b) displays an approximately piecewise linear increase in the downstream direction, with a distinct change in slope occurring at position C in the recompression region for the axisymmetric case, and at position D near the reattachment point for the planar geometry. In these downstream regions, there are fewer but larger turbulent structures in the end views, and so this may lead to the increased shape factor variability. These regions also coincide with the peak Reynolds shear stress locations in the two geometries.[18,22] Thus, the increased levels of shear stress (and general turbulence activity) may lead to a more variable instantaneous shear layer convolution at this location.

Conclusion

The nature of the unsteady motions and interface convolution has been examined in an axisymmetric supersonic separated flow. This study has shown that both flapping (displacement) and area-based pulsing motions along the interface between the freestream and recirculation/wake core regions generally increase in relation to the local shear layer thickness or local enclosed area with increased downstream position. The only exception to this pattern occurs at the mean reattachment point, where fluctuations are somewhat suppressed when compared to adjacent imaging positions. The convolution of the interface between the freestream and recirculating or wake core fluid is also shown to increase with downstream position, with a pronounced increase in the side-view shape factor value between the mean reattachment point and the imaging location in the wake.

Acknowledgments

Funding for this research was provided through the U.S. Army Research Office, Grant DAAG55-97-1-0122, with Thomas L. Doligalski as Technical Monitor.

References

[1]Smith, K. M., and Dutton, J. C., "Investigation of Large-Scale Structures in Supersonic Planar Base Flows," *AIAA Journal*, Vol. 34, No. 6, 1996, pp. 1146–1152.

[2]Bourdon, C. J., and Dutton, J. C., "Planar Visualizations of Large-Scale Turbulent Structures in Axisymmetric Supersonic Separated Flows," *Physics of Fluids*, Vol. 11, No. 1, 1999, pp. 201–213.

[3]Clemens, N. T., and Mungal, M. G., "Two- and Three-Dimensional Effects in the Supersonic Mixing Layer," *AIAA Journal*, Vol. 30, No. 4, 1992, pp. 973–981.

[4]Clemens, N. T., and Mungal, M. G., "Large Scale Structure and Entrainment in the Supersonic Mixing Layer," *Journal of Fluid Mechanics*, Vol. 284, 1995, pp. 171–216.

[5]Messersmith, N. L., and Dutton, J. C., "Characteristic Features of Large Structures in Compressible Mixing Layers," *AIAA Journal*, Vol. 34, No. 9, 1996, pp. 1814–1821.

[6]Dracos, T., Giger, M., and Jirka, G. H., "Plane Turbulent Jets in a Bounded Fluid Layer," *Journal of Fluid Mechanics*, Vol. 241, 1992, pp. 587–614.

[7]Goldschmidt, V. W., and Bradshaw, P., "Flapping of a Plane Jet," *Physics of Fluids*, Vol. 26, No. 2, 1973, pp. 354–355.

[8]Ponton, M. K., and Seiner, J. M., "Acoustic Study of B Helical Mode for Choked Axisymmetric Nozzle," *AIAA Journal*, Vol. 33, No. 3, 1995, pp. 454–462.

[9]Tam, C. K. W., Ahuja, K. K., and Jones, R. R., "Screech Tones from Free and Ducted Supersonic Jets," *AIAA Journal*, Vol. 32, No. 5, 1994, pp. 917–922.

[10]Raman, G., and Rice, E. J., "Supersonic Jet Mixing Enhancement Using Impingement Tones from Obstacles of Various Geometries," *AIAA Journal*, Vol. 33, No. 3, 1995, pp. 454–462.

[11]Smith, K. M., "The Role of Large-Scale Structures in Compressible Reattaching Shear Flows," Ph.D. Dissertation, Dept. of Mechanical and Industrial Engineering, Univ. of Illinois, Urbana, IL, Nov. 1996.

[12]Island, T. C., Patrie, B. J., Mungal, M. G., and Hanson, R. K., "Instantaneous Three-Dimensional Flow Visualization of a Supersonic Mixing Layer," *Experiments in Fluids*, Vol. 20, No. 4, 1996, pp. 249–256.

[13]Sreenivasan, K. R., and Meneveau, C., "The Fractal Facets of Turbulence," *Journal of Fluid Mechanics*, Vol. 173, 1986, pp. 357–386.

[14]Lane-Serf, G. F., "Investigation of the Fractal Structure of Jets and Plumes," *Journal of Fluid Mechanics*, Vol. 249, 1993, pp. 521–534.

[15]Glawe, D. D., Samimy, M., Nejad, A. S., and Chen, T. H., "Effects of Nozzle Geometry on Parallel Injection from the Base of an Extended Strut into a Supersonic Flow," AIAA Paper 95-0522, 1995.

[16]Herrin, J. L., and Dutton, J. C., "Supersonic Base Flow Experiments in the Near Wake of a Cylindrical Afterbody," *AIAA Journal*, Vol. 32, No. 1, 1994, pp. 77–83.

[17]Samimy, M., and Lele, S. K., "Motion of Particles with Inertia in a Compressible Free Shear Layer," *Physics of Fluids A*, Vol. 3, No. 8, 1991, pp. 1915–1923.

[18]Herrin, J. L., and Dutton, J. C., "The Turbulence Structure of a Reattaching Axisymmetric Compressible Free Shear Layer," *Physics of Fluids*, Vol. 9, No. 11, 1997, pp. 3502–3512.

[19]Oh, C., and Loth, E., "A Numerical Investigation of Supersonic Turbulent Shear Layers: Compressibility Effects," AIAA Paper 94-2244, 1994.

[20]Hussain, A. K. M. F., and Zaman, K. B. M. Q., "Vortex Pairing in a Circular Jet under Controlled Excitation. Part 2. Coherent Structure Dynamics," *Journal of Fluid Mechanics*, Vol. 101, No. 3, 1980, pp. 493–544.

[21]Meyer, T. R., Dutton, J. C., and Lucht, R. P., "Vortex Interaction and Mixing in a Driven Gaseous Axisymmetric Jet," *Physics of Fluids*, Vol. 11, No. 11, 1999, pp. 3401–3415.

[22]Amatucci, V. A., Dutton, J. C., Kuntz, D. W., and Addy, A. L., "Two-Stream, Supersonic Wake Flow Field Behind a Thick Base, Part 1: General Features," *AIAA Journal*, Vol. 30, No. 8, 1992, pp. 2039–2046.

M. Samimy
Associate Editor